1488 *Macromolecules* **2010**, *43*, 1488–1498
DOI: 10.1021/ma9024366

Macromolecules
ARTICLE

Strain-Induced Molecular Ordering in Polylactide upon Uniaxial Stretching

G. Stoclet, R. Seguela,* J. M. Lefebvre, S. Elkoun,† and C. Vanmansart

Université de Lille Nord de France, Centre National de la Recherche Scientifique, Université de Lille 1, Unité Matériaux et Transformations, Batiment C6, Cité Scientifique, 59655 Villeneuve d'Ascq, France.
†Present address: Département de Génie Mécanique, Université de Sherbrooke, Sherbrooke, J1K 2R1 Canada.

Received November 4, 2009; Revised Manuscript Received December 18, 2009

ABSTRACT: This study deals with the tensile drawing behavior of a polylactide material containing 4% of D-stereoisomer units, in the amorphous state. The draw temperature domain spanned from the glass transition to the onset of thermal crystallization, namely 70−100 °C. The stress−strain curves exhibit a strain-hardening strongly sensitive to the draw temperature regarding both the onset and the slope of the phenomenon. A detailed structural investigation reveals that various strain-induced phase changes take place depending on the draw temperature. For T_d = 70 °C, a mesomorphic form develops from the strain-oriented amorphous chains, starting at a strain level $\varepsilon \approx 130\%$. In the case T_d = 90 °C, a well-defined crystalline phase grows beyond the strain $\varepsilon \approx 250\%$. In the midtemperature range, i.e. T_d = 80 °C, both the mesomorphic and the crystalline phases are generated in parallel. In all cases, the final weight content of ordered phases at rupture was roughly 30%, irrespective of their form. The observed evolution with increasing draw temperature of the strain-induced structure from mesomorphic to crystalline is quite surprising with regard to the concomitant drop of the strain-hardening. Indeed, if the latter finding is consistent with the thermal activation of plasticity, it also means that the mesomorphic form is almost as much cohesive as the crystalline form in spite of its imperfect ordering. The occurrence of the mesomorphic form is specifically discussed in terms of both chain mobility and thermodynamic metastability.

Introduction

Biosourced polymers have received increasing attention in recent years due to their high potential for packaging applications in substitution to oil-based commodity polymers.[1−5] The biodegradability and biocompatibility of some of these materials is another valuable property. Poly(lactic acid) or polylactide (PLA) is a promising aliphatic polyester, particularly in the field of structural applications. Indeed, regarding thermomechanical properties, PLA can challenge usual commodity plastics.

Polylactide is a broad class of polyesters usually containing both L- and D- stereoisomer units in various amounts due to the tacticity of the methyl side branch every two carbon atoms of the chain backbone. This involves a complex crystallization behavior similar to that random copolymers, including low crystallization kinetics. A good deal of investigations have been focused at understanding the crystallization behavior as a function of molecular architecture, and improving crystallization kinetics via nucleation agents, plasticizers and processing.[6−22]

The improvement of mechanical properties has also been an active investigation area by means of blending with more or less compatible polymers, plasticization, nanofillers[10,14,23−25] including natural nanoparticles issued from biomass.[26,27] The issue of most of these attempts was rather modest in terms of mechanical performances if not detrimental, so far. In contrast, the structural evolution of PLA upon stretching and the accompanying changes in mechanical behavior have been scarcely addressed.[28−33] This is of prime concern for understanding the structure−property relationships of PLA and optimizing the use properties via processing.

Structural studies of oriented pure poly(L-lactide), namely PLLA, revealed that strain-induced crystallization is straightforward upon drawing above the glass transition temperature. Moreover, it was shown that depending on the drawing conditions, PLLA is able to crystallize into different forms. The α crystal form, first described by De Santics and Kovacs[34] as an orthorhombic unit cell with 10/3 helix chain conformation, was later refined by Hoogsteen and co-workers.[35] This crystal form, which is the most thermodynamically stable one, can be obtained by stretching at low draw rate and low draw temperature[35] or by quiescent isothermal crystallization above 120 °C.[36] Zhang et al.[36] have also reported a defective α' form via quiescent crystallization below 120 °C. The β crystal form is obtained under tensile drawing at high stretching rate and high draw temperature. This crystal form was first reported by Eling and co-workers[37] and later identified by Hoogsteen et al.[35] as orthorhombic with 3/1 helix chain conformation. Puiggali et al.[38] more recently suggested a trigonal structure with frustrated stacking of 3-fold helices accounting for the accommodation of the random up−down orientation in the crystal of neighbor chains associated with rapid crystallization conditions.

More recently, Mulligan and Camak[29] reported the occurrence of a nematic-like order upon drawing a polylactide with 2% D-isomer just above its glass transition temperature using X-ray scattering and birefringence measurements. No quantitative data were yet provided regarding this kind of liquid-crystal form.

In a previous paper,[31] we reported on the crystallization kinetics and the preliminary study of the uniaxial and biaxial drawing of a PLA material containing 4.3 mol % of D-stereoisomer. The present study focuses on the structural evolution of this material as a function of strain and draw temperature under uniaxial testing by means of quantitative X-ray scattering analysis. The mechanism of the strain-induced phase changes is also discussed.

*Corresponding author. E-mail: roland.seguela@univ-lille1.fr.

 Published on Web 01/05/2010

Experimental Section

Material and Preparation. The polylactide (PLA) of the study is the 4042D grade material from Natureworks (USA) containing 4.3 mol % of D-isomer units. The number-average and weight-average molar weights are M_n = 116 kDa and M_w = 188 kDa, respectively, as determined from size exclusion chromatography. PLA films were coextruded between two layers of low density polyethylene using a film blowing line equipped with three single screw extruders. Details on the experimental procedure are described elsewhere.[31] The 200 μm thick PLA layer was easily peeled off from the two polyethylene layers owing to a very weak adhesion energy. In order to remove internal stresses due to the extrusion process, and to erase physical aging, the PLA films were systematically annealed at 70 °C, i.e. $T_g + 10$ °C, during 15 min and slow cooled down to room temperature (RT) before every experiment. Undetectable dimensional changes during annealing indicated that the films were already isotropic after processing. Moreover, observation between cross-polarizers revealed total relaxation of internal stresses.

Mechanical Behavior. Uniaxial tensile deformation was carried out using an Instron machine Model 4466 equipped with an environmental chamber. The dumbbell specimens having 22 mm and 5 mm in gauge length and width were strained at a constant crosshead speed of 50 mm/min, i.e. an initial strain rate $\dot{\varepsilon} = 4 \times 10^{-2}$ s^{-1}. Five specimens were tested for every experimental condition. The samples were rapidly cooled down to RT under tension prior to unloading in order to prevent relaxation and structure evolution for further *ex situ* characterization of the deformed samples. Ink marks printed at intervals $l_o \approx 2$ mm along the sample length prior to drawing enabled determining the local strain, $\varepsilon = l/l_o$, True stress - true strain measurements were performed using a video-controlled extensometer. Longitudinal and transverse strains were determined from a seven point grid printed on the sample. The true stress, σ, is the ratio of the force to the actual cross section area of the sample assuming transverse isotropy of the deformation through the width and thickness, according to *ex situ* measurement. The true strain is taken as the longitudinal local strain, ε, as defined above.

DMA Measurements. A RSA3 apparatus from TA Instrument was used for Dynamic Mechanical Analysis (DMA). Experiments were performed at a frequency of 10 Hz in the temperature range 25−100 °C. The dynamic strain amplitude, $\varepsilon_o = 0.4 \times 10^{-3}$, was determined after preliminary measurement of the strain domain for which the material obeys linear viscoelasticity.

DSC Measurements. Differential Scanning Calorimetry (DSC) was performed on a Perkin-Elmer DSC7 apparatus. Samples of about 10 mg inserted into aluminum pans were scanned at a heating rate of 10 °C/min under nitrogen gas flow. The temperature and heat flow scale were calibrated using a high purity indium and zinc samples according to standard procedures. The crystalline weight fraction was computed from the enthalpy of the melting exotherm using the specific enthalpy of fusion of the perfect crystal $\Delta H_f° \approx 94$ J/g after Fischer et al.[39] This data is the one most frequently used, so that it allows making comparison between various studies. However, it is worth noticing a more recent value reported by Jamshidi et al.[40] that is about twice as large. In the case of partially crystallized drawn samples, the crystallinity index was determined by subtracting the enthalpy of cold-crystallization from the total melting enthalpy.

WAXS Measurements. Wide-angle X-ray scattering (WAXS) analysis was carried out owing to a Rigaku rotating anode equipment operating at 50 kV and 100 mA. The Cu Kα radiation (λ = 1.54 Å) was selected with a point focusing monochromator. The WAXS patterns were recorded on MAR2300 imaging plates. Through-view and edge-view 2D-patterns revealed cylindrical symmetry for all drawn samples, so that 180°-azimuthal integration by means of the FIT2D software of the through-view patterns only could be used for quantitative assessment of the various phases. The WAXS intensity profiles were further treated using the PeakFit software, assuming Gaussian profiles for all scattering peaks and amorphous halo. The weight fraction of the various phases was computed from the ratio of the specific scattering contribution of every one to the total scattering area. For the sake of clarity, some of the reported intensity profiles have been restricted to the $5° < 2\theta < 30°$ range. Quantitative calculations have been however carried out over the whole scattering spectrum $5° < 2\theta < 45°$.

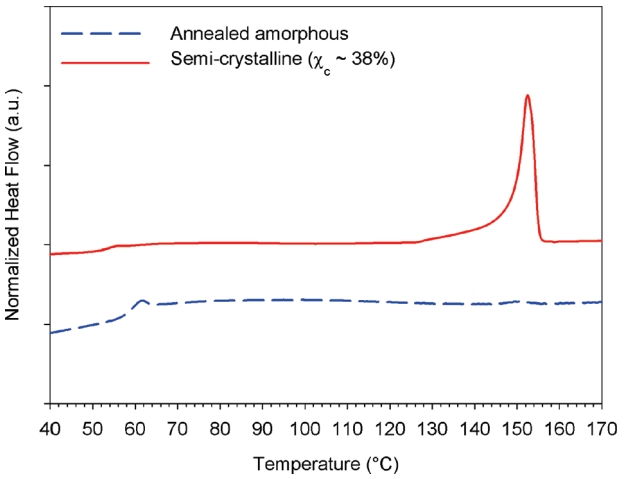

Figure 1. DSC heating scans of samples of the blow-extruded PLA film: (a) after annealing at 70 °C for 15 min and (b) after isothermal crystallization at 105 °C for 2 h.

Several procedures have been proposed for computing the mesomorphic phase fraction in polyesters from WAXS[41−43] assuming the knowledge of the crystalline and amorphous scattering contributions. In the present study, the amorphous WAXS intensity profile is first experimentally identified from the scattering pattern of the thoroughly amorphous film sample. Samples drawn at high temperature enabled identifying the strain-induced crystalline contribution, which was close to that reported for the α' form. In this case, the presence of distinct sharp peaks made it easier the PeakFit treatment by fixing the position of the various peaks, only their full width at half-maximum (FWHM) and intensity being let self-adjusting. Samples drawn just above the glass transition temperature (T_g) made it possible identifying the mesomorphic form contribution owing to no trace of crystal scattering. In this case, only humps appeared on the amorphous halo so that the PeakFit treatment was let free to self-adjust the position, intensity and FWHM of a new peak. Validation of the method was provided by the fact that applying the same procedure to several samples having various plastic strains resulted in the same scattering profile for the mesomorphic phase, except for the intensity. An additional support to the mesomorphic phase identification was *a posteriori* afforded by comparison of the FWHM data of the various components.

Results

Thermal and Mechanical Behavior. Figure1 shows the DSC heating trace of the annealed PLA film. This sample exhibits a glass transition temperature $T_g \approx 58$ °C and a broad cold crystallization exotherm in the temperature range 110−145 °C. The crystallinity $X_c < 1\%$ computed from the faint melting peak around 150 °C reveals (1) that the present PLA has either very low crystallization kinetics or low crystallization capability and (2) that the as-blown films are thoroughly amorphous. Figure 2 reports the crystallinity versus temperature for various durations of isothermal crystallization. It appears that, even at the optimum

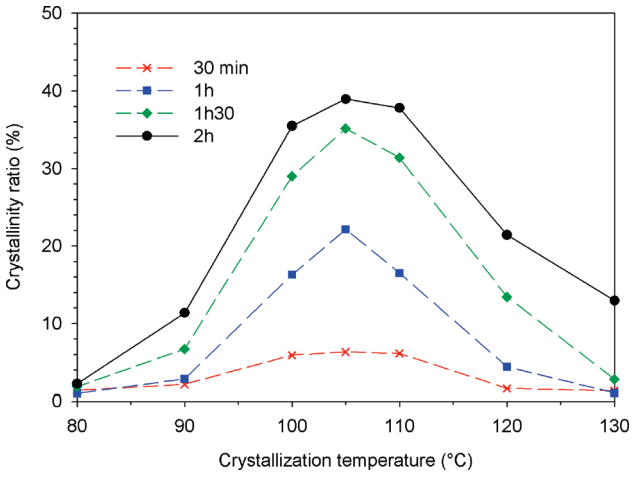

Figure 2. Crystallinity index of PLA versus isothermal crystallization temperature for various elapsed times.

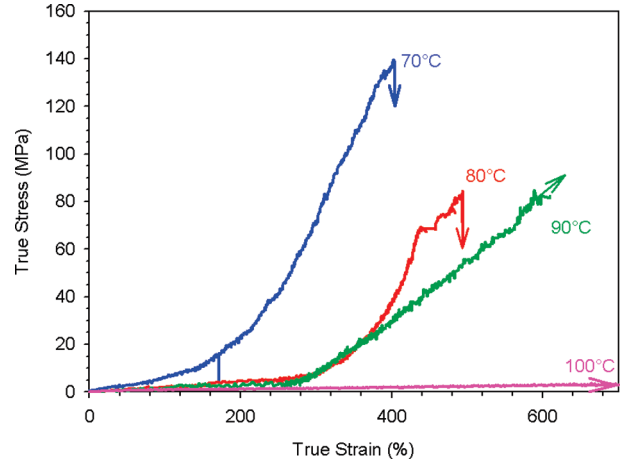

Figure 3. True stress−true strain curves of PLA films at various draw temperatures beyond the glass transition temperature.

crystallization temperature T_c = 105 °C, several hours are required for the crystallization completion. The crystallinity index can yet reach a relatively high level $X_c \approx 40\%$. The DSC heating curve of a sample isothermally crystallized at 105 °C for 2 h (Figure 1) displays a very sharp melting peak which contrasts with the DSC heating scan of the sample annealed at 70 °C. Regarding uniform cooling from the melt, the previous study showed that significant crystallinity (X_c > 20%) can only be obtained if the cooling rate is lower than 0.5 °C/min.[31]

Figure 3 reports the true stress−true strain curves upon uniaxial tensile drawing of PLA film samples as a function of the draw temperature above the glass transition temperature. PLA displays a rubber-like behavior up to a strain $\varepsilon \approx 130\%$ for T_d = 70 °C, or $\varepsilon \approx 250\%$ for $T_d \geq 80$ °C. Beyond the critical strain level for every draw temperature, strain-hardening takes place. This mechanical behavior is similar to that of amorphous PET for which it has been assigned to the strain-induced crystallization beyond a critical level of chain orientation.[44,45] It is noteworthy that the slope, $\partial\sigma/\partial\varepsilon$, of the strain hardening of PLA is strongly dependent on the draw temperature, the higher the temperature the softer the strain-hardening. This general trend regarding semicrystalline polymers is relevant to the decay of the strength of molecular interactions with increasing temperature which results in improved plasticity.[46−50] In the present case of PLA having very slow crystallization rate and displaying polymorphism, the temperature-dependence of the crystallization kinetics and the nature of the strain-induced structure may also have an influence on the strain-hardening evolution. This point will be addressed in the next section.

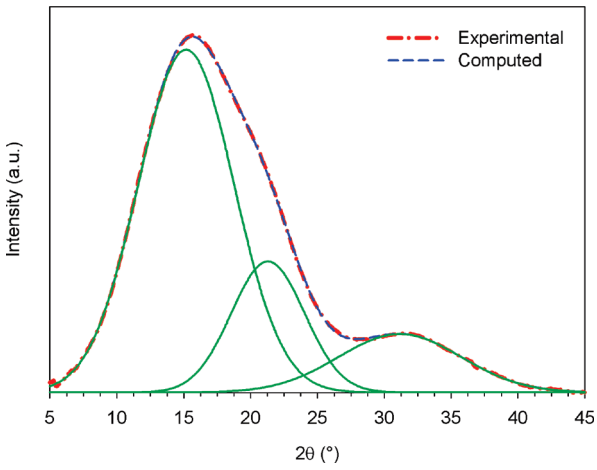

Figure 4. WAXS intensity profile of the blow-extruded and annealed PLA film.

For T_d = 100 °C, PLA deforms like an un-cross-linked elastomer with no strain-hardening up to rupture. The drawing looks like melt spinning, accompanied by an extremely large deformation exceeding 750% (the sample does not break within the limit of crosshead displacement of the tensile machine). This observation, already reported by Mahendrasingam et al.,[51] suggests that strain-induced crystallization cannot occur under the experimental conditions T_d = 100 °C and $\dot{\varepsilon} = 4 \times 10^{-2}$ s^{-1}. It is suspected that chain relaxation is much faster than chain extension. This assumption will be discussed further.

WAXS Study. *Blown Films.* Figure 4 shows the WAXS intensity profile of the blow-extruded and annealed PLA film that stands for the amorphous material, according to DSC. The fitting procedure reveals three halos located at 2θ = 15.0°, 2θ = 21.2° and 2θ = 31.0°, with roughly equal FWHM ≈ 8°. The merging of the first two halos results in a broad scattering similar to the case of PET, as shown by Murthy et al.,[41] who suggested two interchain distances. Borrowing from this analogy, one may suspect two characteristic interchain spacings in amorphous PLA, considering in addition that intrachain spacings in amorphous polymers are generally largely different from the interchain ones.[52] This point will be discussed in the next subsection.

Drawing at T_d = 70 °C. Figure 5 displays the 2D-WAXS patterns of samples drawn at T_d = 70 °C, at strains of 130% and 360%, i.e., before and within the strain hardening domain, respectively. The diffuse halo of the WAXS pattern at ε = 130% exhibits a slight reinforcement on the equator, indicating an orientational trend of the chains in the drawn direction. At ε = 360%, the WAXS pattern displays a very strong equatorial reinforcement of the halo relevant to a very high degree of chain orientation. It is worth noticing that the continuous intensity decrease of the inner broad scattering on the meridian and the concomitant intensity increase on the equator with increasing draw ratio confirms the previous assumption that both components at 2θ = 15.0° and 2θ = 21.2° arise from interchain spacings. In contrast, the meridian reinforcement of the third amorphous scattering located at $2\theta \approx 31°$ gives clear evidence of an intrachain spacing d ≈ 0.29 nm along the chains, that is precisely the characteristic distance between the methyl groups in the

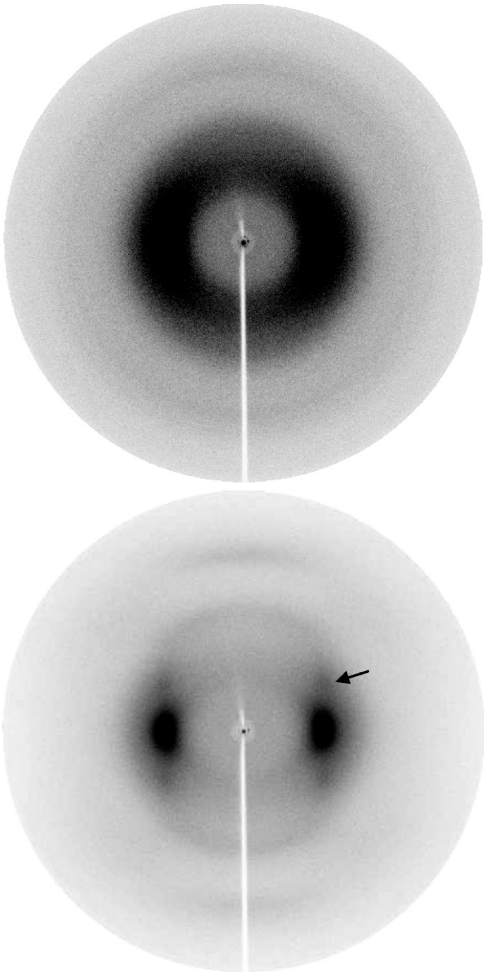

Figure 5. 2D-WAXS patterns of PLA samples drawn at T_d = 70 °C: (a) ε = 130%; (b) ε = 360% (arrow indicates a very faint (203) reflection from the α′ crystal form).

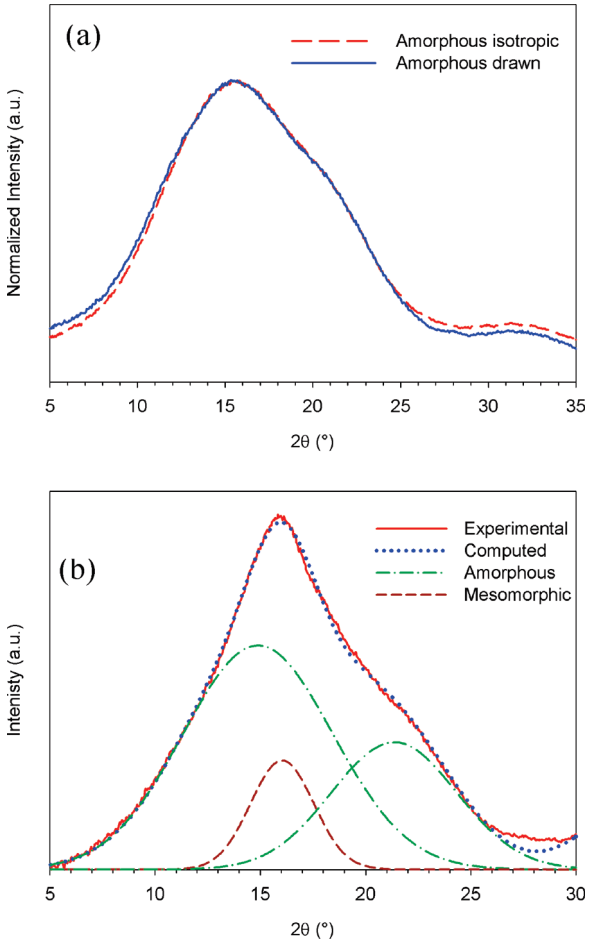

Figure 6. WAXS intensity profiles of PLA samples drawn at T_d = 70 °C: (a) ε = 130% and (b) ε = 360% (azimuthal integrations of the 2D-patterns of Figure 4). Also shown in part a is the intensity profiles of the isotropic blown film for comparison.

3-fold helices. Pluta and Galeski[32] have formerly assigned this kind of meridian scattering to the development of crystallinity upon plastic deformation of a polylactide having 30% of D-isomer units, considering that it did not exist for the isotropic amorphous material. In the present case, the assignment of the scattering at $2\theta \approx 31°$ to an amorphous contribution is quite obvious from the intensity profile of the amorphous material (Figure 4) and the 2D-pattern prior to the onset of strain-induced crystallization (Figure 5a).

Figure 6 shows the azimuth-integrated intensity profiles of the patterns of Figure 5. For ε = 130%, the intensity profile is very close to that of the isotropic amorphous film (Figure 6a). This means that the material drawn at T_d = 70 °C is still amorphous at a strain of 130%, and that the overall interchain spacing distribution is not affected by stretching. Thereby, the azimuth-integrated profile of Figure 4 will be taken as the amorphous scattering contribution in all further treatments of WAXS intensity profiles and calculations of phase concentrations.

Regarding the intensity profile of Figure 6b for the strain ε = 360%, an additional contribution at 2θ = 16.2° with FWHM ≈ 3.5° was required for fitting the experimental data. The same procedure had to be applied for all samples drawn at T_d = 70 °C for strains beyond 100%, i.e., in the strain-hardening domain.

Figure 7 shows that the FWHM of the additional scattering contribution not only is independent of strain but is also twice as small as that of the main amorphous halo. This is

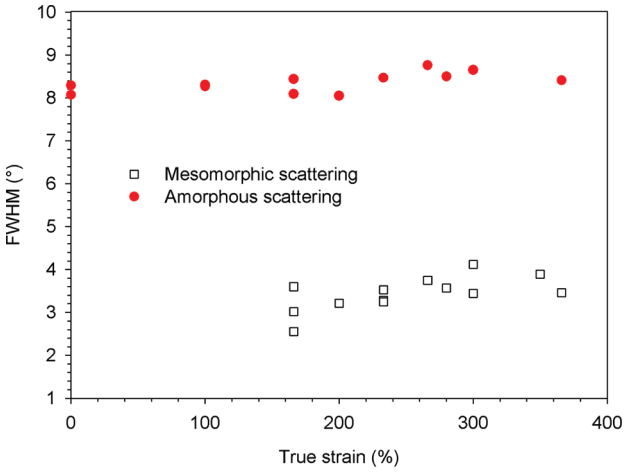

Figure 7. FWHM versus plastic strain of the main amorphous scattering located at 2θ = 15.5° and of the mesomorphic scattering located at 2θ = 16.2°.

evidence that a new state of order as grown in the drawn material. Its characteristic FWHM suggests an intermediate ordering between crystal and amorphous, namely a mesomorphic form or mesophase. Mulligan and Cakmak previously claimed that a nematic order builds up, as judged from the high chain orientation without 3D-ordering.[29] In the present case, the shift of the mesomorphic scattering to

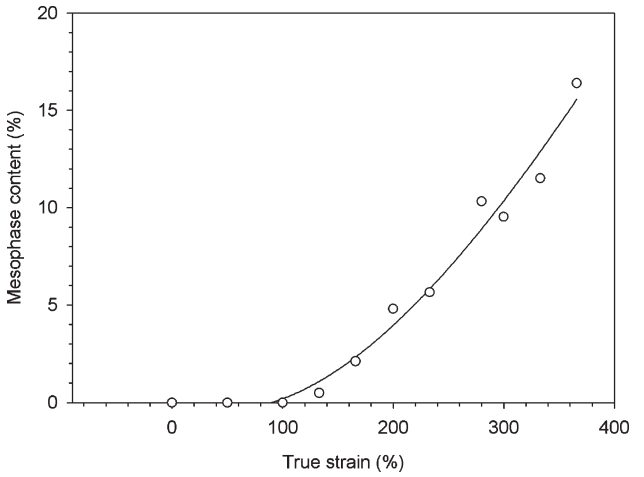

Figure 8. PLA mesomorphic phase fraction versus plastic strain for $T_d = 70$ °C.

higher angle with regard to the main amorphous halo, namely $2\theta = 16.2°$ versus $2\theta = 15.0°$, means that the average interchain distance in the mesomorphic form is substantially reduced with regard to the most probable spacing of the amorphous chains. This reinforces the previous conclusion from the FWHM data of an increased chain ordering but not necessarily the nematic-like order. A direct conclusion from the mesomorphic WAXS characteristics is that both chain packing and chain interactions are somewhat higher than in the amorphous state.

One may wonder if the strain-induced phase does not just consist of very small or highly defective α′ crystals that would indeed involve both 2θ shift of the main crystalline reflection and intermediate FWHM between amorphous and crystalline states. The absence of off-equator reflections in the WAXS patterns of samples drawn at $T_d = 70$ °C is a hint in favor of only lateral chain ordering that supports mesophase instead of highly defective crystals. However, at the strain $\varepsilon = 360\%$ close to rupture, the occurrence of a very weak and diffuse scattering about the location expected for the (203) reflection reveals first clues of α′ crystal ordering (see the arrow in Figure 5b).

Figure 8 reports the evolution with strain of the mesomorphic component at the draw temperature $T_d = 70$ °C. Within the experimental accuracy, the onset of growth of the mesomorphic phase appears at $\varepsilon = 130 \pm 20\%$ that is close to the onset of strain-hardening on the stress−strain curve of Figure 3. This correspondence is clearly relevant to the incidence of the strain-induced phase transformation on the mechanical behavior. It also means that the mesomorphic phase is much more cohesive than the amorphous phase just above T_g so that the growth of mesomorphic microdomains results in an increasing density of physical cross-links in the rubbery amorphous material. The previous observation that the average interchain distance is significantly lower in the mesomorphic state as compared with the amorphous state is a strong clue in support to a greater cohesiveness of the former phase.

Drawing at $T_d = 90$ °C. The 2D-WAXS patterns regarding the drawing at $T_d = 90$ °C are reported in Figure 9 as a function of strain. At the strain $\varepsilon = 100\%$, the material looks completely amorphous with a very slight orientation of the chains parallel to the draw direction. The chain orientation is noticeably lower than at the draw temperature $T_d = 70$ °C at equivalent strain (Figure 5) due to significant chain relaxation during the time scale of the drawing, as previously suggested by Mahendrasingam et al.[51] Then, at $\varepsilon = 170\%$, faint but clear-cut crystalline reflections appear on the equator and at off-equator positions. These first signs of strain-induced crystallization appear at significantly lower

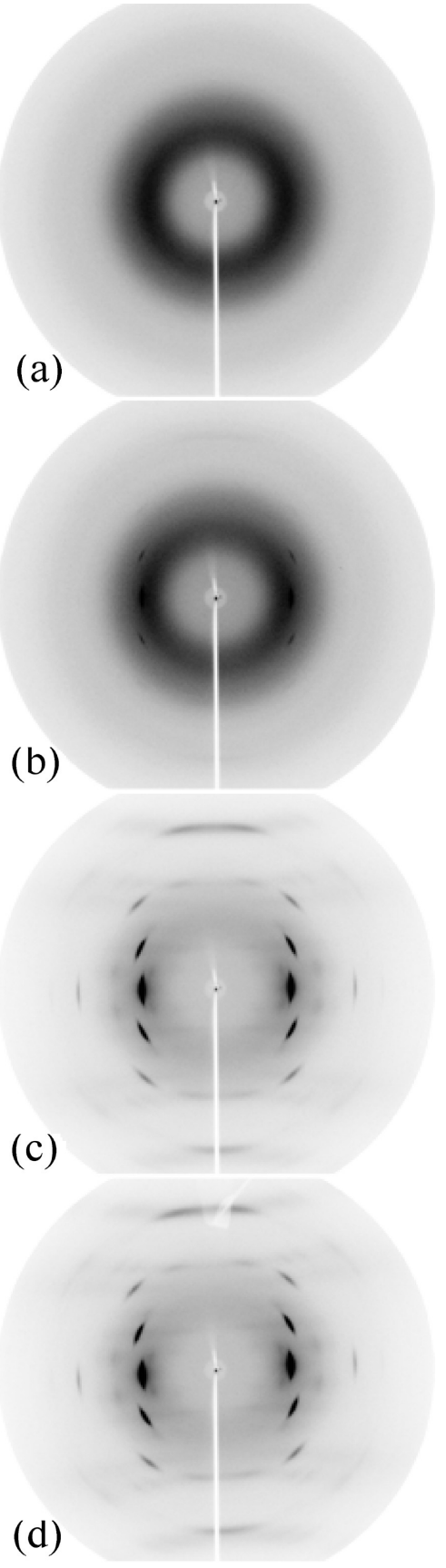

Figure 9. 2-WAXS patterns of PLA samples drawn at $T_d = 90$ °C: (a) $\varepsilon = 100\%$; (b) $\varepsilon = 170\%$; (c) $\varepsilon = 330\%$; (d) $\varepsilon = 400\%$.

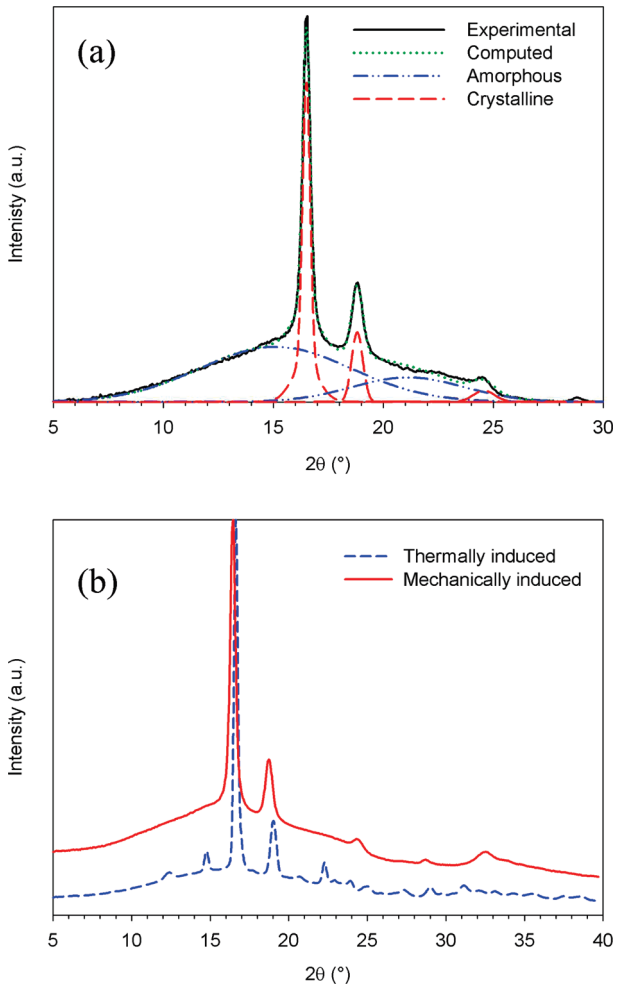

Figure 10. WAXS intensity profile of a PLA sample drawn to ε = 230% at T_d = 90 °C (azimuthal integration of the 2D-pattern of Figure 8c): (a) curve-fitting analysis; (b) comparison with the WAXS intensity profile of a sample isothermally crystallized at 105 °C for 2 h.

strain than the strain-hardening threshold, which suggests that a sufficient volume fraction of crystallites is required to build up the physically cross-linked network that triggers strain-hardening. Drawing far beyond 170% (Figure 9, parts c and d) gradually promotes the growth of crystalline phase with a strong fiber texture. The remaining amorphous phase still displays a rather low chain orientation, as revealed by the nearly uniform intensity of the amorphous halo. This is a hint that strain-induced crystallization develops when the most oriented chain reach a critical orientation level, as previously suggested form the mechanical behavior.

The azimuth-integrated intensity profiles of various drawn sample have been successfully curve-fitted with amorphous and crystalline contributions. Owing to their sharpness, the later ones were easily characterized by their scattering position and FWHM parameters. The crystalline FWHM ≈ 0.5° is much lower than that of the mesomorphic reflections (Figure 9). An example of analysis of the WAXS intensity profile is reported in Figure 10a for the sample drawn at ε = 330%. Not any mesomorphic contribution was needed for curve-fitting the experimental data, irrespective of the strain level. Comparison of the intensity profile of the drawn sample with that of a sample isothermally crystallized at T = 105 °C for 2 h is shown in Figure 10b. The latter profile is characteristic of the orthorhombic α form of PLA while the former one is typical of the α′ crystal form, the

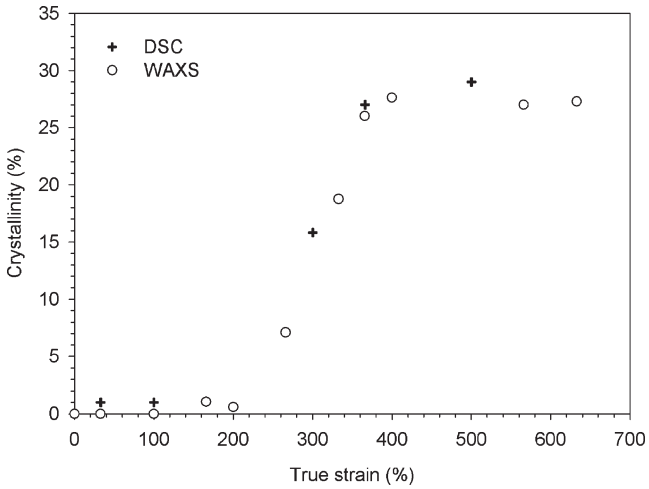

Figure 11. PLA crystalline phase fraction versus plastic strain for T_d = 90 °C (data from DSC are also reported).

distorted parent of the α form described by Zhang et al.[35] Indeed, the slight shift to lower scattering angle of the strong (200)/(110) and (203) reflections located at $2\theta \approx 16.7°$ and $2\theta \approx 19.1°$, respectively, together with the absence of the (010) and (210) reflections at $2\theta \approx 14.8°$ and $2\theta \approx 22.2°$ give evidence of some disorder in the chain packing of the orthorhombic α unit cell.

The absence of the mesomorphic form irrespective of the strain level at T_d = 90 °C indicates that this imperfectly ordered form is thermodynamic unstable at 90 °C and suggests that the energy barrier to the strain-induced crystallization is much lower at 90 °C than at 70 °C due to increased chain mobility.

Figure 11 reports the crystal fraction evolution with plastic strain at T_d = 90°. The WAXS data compare quite well with the DSC data. The shorter strain domain in which the disorder−order transition occurs, as compared with 70 °C (Figure 7), supports the previous assumption that the mechanism of strain-induced molecular ordering is much easier at 90 °C, particularly from a kinetics standpoint. It is also noteworthy that the crystallinity level actually jumps at $\varepsilon \approx$ 250% (Figure 11) that is better consistent with the onset of the strain-hardening at the same draw temperature (Figure 3) than the first hints of crystallization pointed out at ε = 170% (Figure 9).

The previous observation (Figure 3) that the strain-hardening is softer at T_d = 90 °C than at T_d = 70 °C is consistent with the concept of thermally activated plasticity. However, it is quite surprising in consideration that the strain-induced phase at T_d = 90 °C is actually crystalline whereas it is mesomorphic for T_d = 70 °C. This means that, in spite of a defective ordering, the mesomorphic form is almost as much cohesive as the crystalline form.

The shift of the onset of the strain-induced disorder−order transition to higher strain when T_d increases from 70 (Figure 8) to 90 °C (Figure 11) is an additional evidence of the previously mentioned improvement of chain relaxation that parallels the increased chain mobility. Indeed, owing to chain relaxation, the chain orientation rate drops at T_d = 90 °C, so that higher strain should be applied to reach the critical chain orientation required for the disorder−order transition. However, it should be pointed out that if the increase of draw temperature is detrimental for the chain orientation process, it is beneficial for both the degree of molecular ordering (crystalline versus mesomorphic) and the kinetics of the strain-induced phase transition (reduced strain-domain).

Drawing at T_d = 80 °C. Figure 12 shows 2D-WAXS patterns at various strains recorded for the drawing at T_d = 80 °C. At first sight, these patterns look similar to the ones recorded for the drawing at T_d = 90 °C, i.e. the amorphous chain are gradually oriented prior to the occurrence of the strain-induced crystallization beyond a strain ε = 160%. The azimuth-integrated intensity profiles provide better insight into the strain-induced structural changes. Figure 13 is an example of intensity profile for the sample drawn at ε = 230% which displays clear-cut crystalline reflections. Applying the curve-fitting procedure yet revealed that amorphous and crystalline contributions could not account for the whole scattering. It was necessary to introduce a mesomorphic contribution borrowed from the study of the drawing at T_d = 70 °C.

Figure 14 reports the evolution with strain of the weight fraction of the three phase. The more complex curve-fitting procedure used in the present instance resulted in greater standard deviation of the data. The onset of the strain-induced disorder−order transition is not so clear than for the two previous cases of drawing at T_d = 70 °C and T_d = 90 °C which involved only one of the two ordered forms, i.e. either the mesomorphic or the crystalline form. Besides, it is not possible to establish which of the mesomorphic or the crystalline form appears first. Notwithstanding, Figure 14 shows that the disorder−order transition occurs in the strain range 160−200%, and the fractions of the mesomorphic and the crystalline phases increase roughly in parallel up about 15%. The total fraction of the two ordered phases reaches a maximum value of about 30% that is not far different from the maximum fraction of either the mesomorphic or the crystalline phase at T_d = 70 °C and T_d = 90 °C, respectively.

Drawing at T_d = 100 °C. The WAXS study of the samples drawn at T_d = 100 °C reveals no strain-induced crystallization over the whole strain range. The 2D-pattern of Figure 15 for a sample drawn up to ε = 600% does not display any signs of crystalline reflections. Besides, the amorphous halo is quite isotropic. These findings corroborate the previous assumption from the mechanical behavior that chain relaxation is much faster than chain extension for the applied strain-rate 4×10^{-2} s^{-1} at 100 °C, so that strain-induced crystallization is unable to take place. It is also worth reminding that thermal crystallization as well cannot occur during drawing due to the very low kinetics of PLA quiescent crystallization at 100 °C (Figure 2).

About the PLA Mesomorphic Form. A metastable mesomorphic form at RT is not specific to polylactide. Indeed, a number of aromatic polyesters such as PET,[41,42,53−60] poly(ethylene−naphthalate),[55,56,61−63] poly(trimethylene−terephthalate),[64] poly(butylene−terephthalate),[65] poly(esteramides),[66] and a number of semicrystalline polymers such as polypropylene, nylons and ethylene/vinyl−alcohol copolymers (see ref 67. and the references cited therein) have been reported to develop a mesomorphic order upon either drawing at temperature far below the melting point or rapid cooling from the melt, in some instances. The occurrence of such an imperfectly ordered state in polylactide has been speculatively ascribed by Mulligan and Cakmak[29] to the noncomplete achievement of the main mechanical relaxation in the temperature window of the experiments that impedes the chain arrangement into a crystallographic register. Figure 16 displays the storage and loss moduli versus temperature of the PLA material of the study, at a 10 Hz frequency that roughly corresponds to the midvalue of the strain-rate range of the drawing experiments ($4 \times 10^{-2} > \dot{\varepsilon} > 8 \times 10^{-3}$ s^{-1} over the whole strain domain at constant crosshead speed). Indeed, the average strain rate in DMA experiments

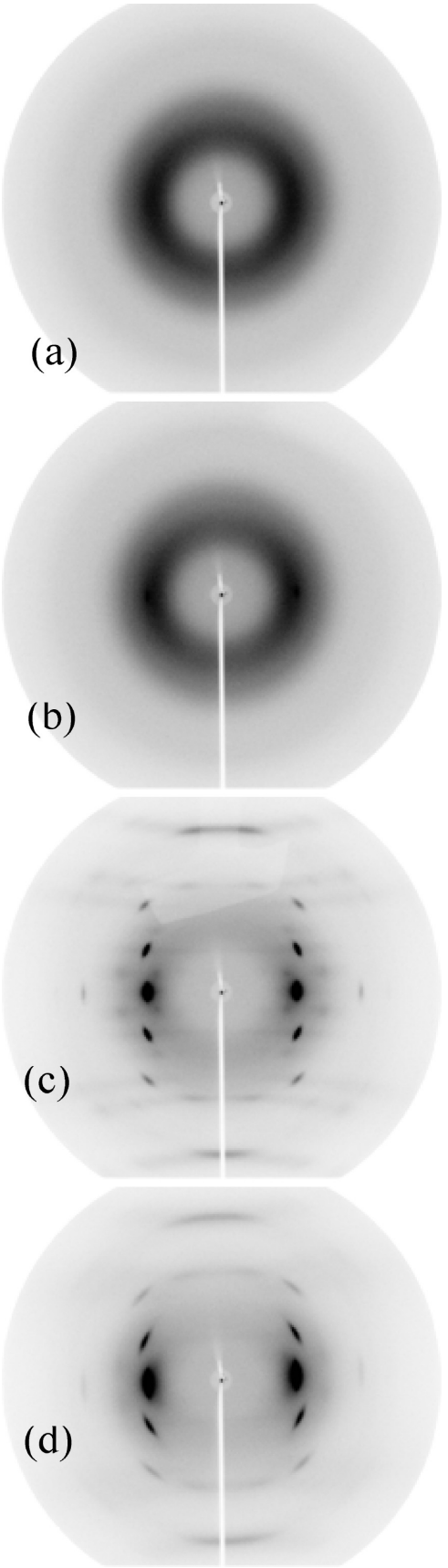

Figure 12. 2D-WAXS patterns of PLA samples drawn at T_d = 80 °C: (a) ε = 100%; (b) ε = 160%; (c) ε = 230%; (d) ε = 400%.

can be estimated from the following relation $\dot{\varepsilon} = 4\varepsilon_o/T$ where $\varepsilon_o = 0.4 \times 10^{-3}$ is the strain amplitude of the periodic

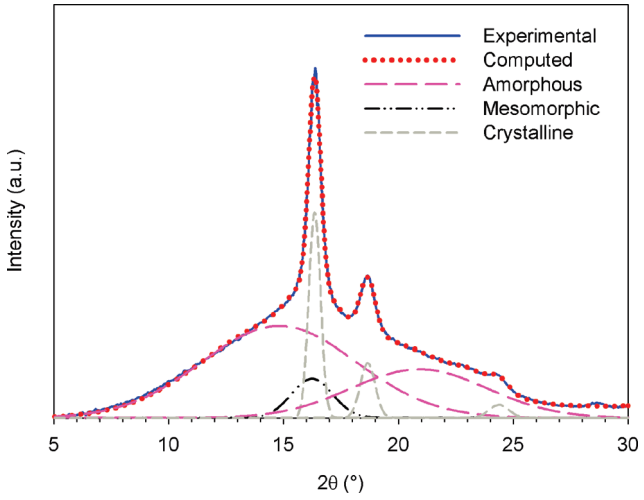

Figure 13. WAXS intensity profile of a PLA sample drawn to ε = 230% at T_d = 80 °C (azimuthal integration of the 2D-pattern of Figure 12c).

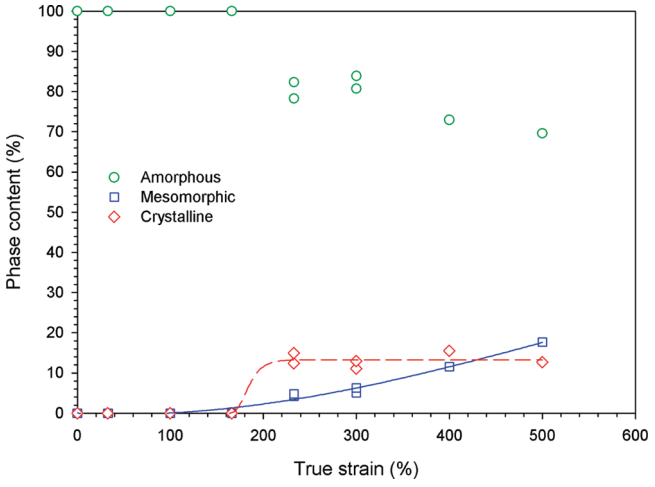

Figure 14. Evolution with plastic strain of the PLA amorphous, mesomorphic and crystalline weight fractions for T_d = 90 °C.

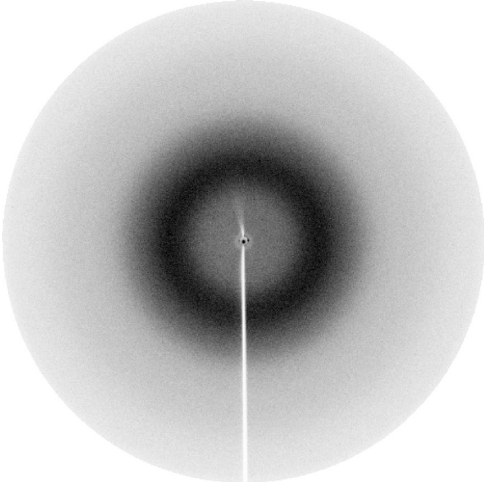

Figure 15. 2D-WAXS patterns of PLA drawn to ε = 600% at T_d = 100 °C.

deformation and $T/4$ is the quarter period of the oscillation.[68,69] According to the storage modulus data, PLA was in

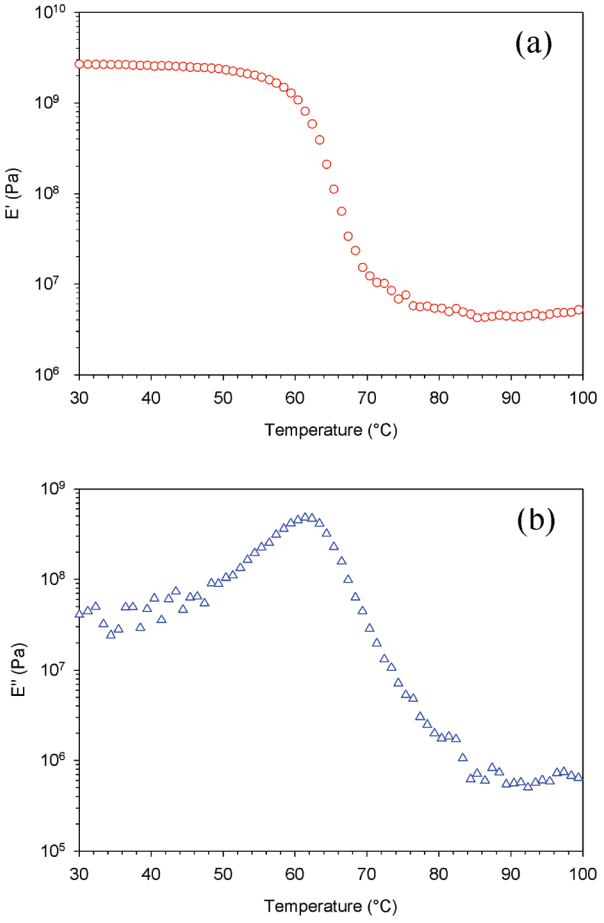

Figure 16. Storage and loss moduli of PLA versus temperature at 10 Hz frequency.

the rubbery state for all experiments performed in the draw temperature range 70−90 °C. In contrast, the loss modulus was roughly 50 times greater at 70 °C than at 90°. This means that the amorphous chains suffered much more from chain relaxation ability during the drawing at T_d = 70 °C than at T_d = 90 °C. This is in perfect agreement with Mahendrasingam et al.[51] hypothesis that the relaxation of the chains in the temperature range just above the glass transition governs the strain-induced crystallization, as formerly demonstrated in the case of PET,[70] although the former authors did not report on the occurrence of a mesomorphic order in PLA. The broader strain domain over which the amorphous-mesomorphic transition occurs at T_d = 70 °C (Figure 8) as compared with that of the amorphous−crystal transition at T_d = 90 °C (Figure 11) is also a hint of reduced molecular mobility in the former case.

It is worth noticing that most of the polymers which display a mesomorphic order do not exhibit a specific mechanical relaxation in the temperature range where a mesomorphic form is well-known to occur, in particular polyesters. Only polypropylene and ethylene/vinyl alcohol copolymers do exhibit a well-defined mechanical relaxation (far above the main relaxation of the amorphous phase) to which the stability of the mesomorphic structure can been related.[67] Therefore, if chain relaxation was the major factor for the generation of a strain-induced mesomorphic order, all semicrystalline polymers should be potentially able to exhibit a mesomorphic form under appropriate drawing conditions, which is not the case. In the present instance of PLA, lacking molecular mobility only cannot account for the buildup of a mesomorphic order characterized by

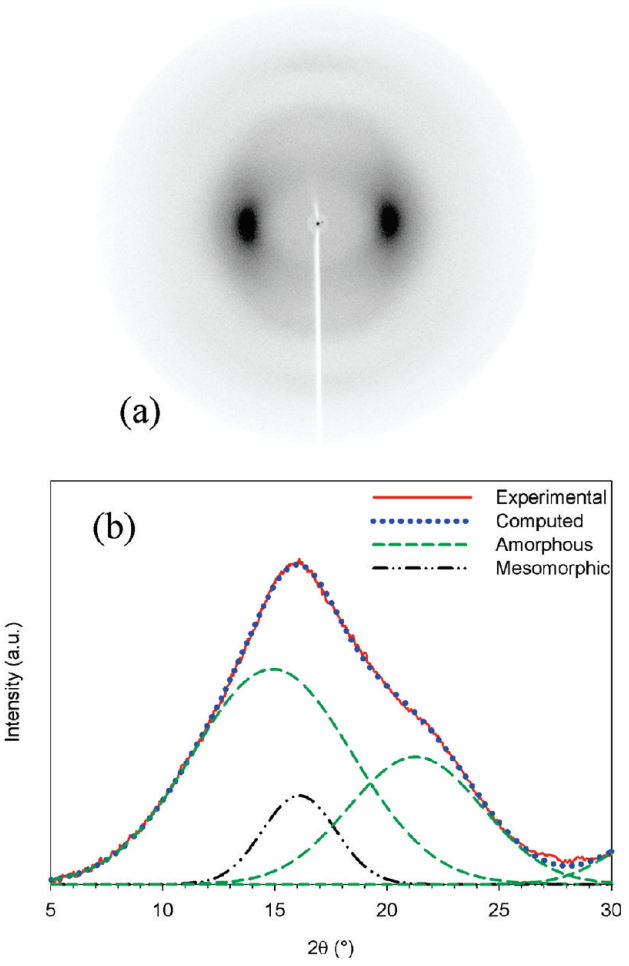

Figure 17. X-ray scattering of PLA drawn to $\varepsilon = 230\%$ at $T_d = 35$ °C: (a) 2D-WAXS pattern; (b) curve-fitting of the azimuth-integrated profile.

a well-defined X-ray scattering located at $2\theta = 16.2°$ with a rather narrow FWHM $\approx 3.5°$, irrespective of draw temperature and strain level. Furthermore, the strain-hardening accompanying the development of the mesomorphic form at $T_d = 70$ °C is relevant to a strong cohesion of the strain-induced structure, i.e. an evidence of strong intermolecular interactions in spite of the defective ordering. This suggests that specific structural factors and chain interactions are also involved in the process. This means that thermodynamics is a contributing factor in parallel with chain mobility, after Wunderlich et al.[71,72] regarding the occurrence of a mesomorphic order in polymers in a general sense.

It is worth having a look at the drawing behavior of amorphous PLA at temperatures below 70 °C. In contrast to the drawing in the rubbery state, the deformation in the glassy state turns gradually heterogeneous when T_d is decreased below T_g: a plastic instability develops accompanied by a diffuse neck which becomes sharper with decreasing T_d. However, a partial structural transition into the mesomorphic form invariably occurs for any draw temperature. For example, Figure 17a shows the 2D-WAXS pattern of PLA drawn at 35 °C up $\varepsilon = 160\%$ (in the necked region). The pronounced equatorial reinforcement of the main scattering halo is relevant to the strong molecular orientation in the draw direction, at similar level as in the case $\varepsilon = 160\%$ for $T_d = 70$ °C (Figure 5b). However, there is no hint of off-equatorial scattering associated with the (203) α' reflection. The curve-fitting analysis of the azimuth-integrated intensity profile reported in Figure 17b reveals the presence of the mesomorphic scattering, though most of the materials is still amorphous. The fact that a significant amount of mesomorphic form develops at large strains whatever the draw temperature 25 °C $< T_d <$ 70 °C means that the phenomenon is not much sensitive to the relaxation time distribution of the amorphous chains that should drastically change over the whole temperature range (note that the self-heating in the plastic instability for the strain rate of the present study does not exceed a few degrees for a 200 μm thick film). In other words, molecular mobility is not the only factor that governs the growth of the mesomorphic form. Thermodynamics obviously play a determining role via specific chain interactions that build up during the drawing process, benefiting from the strain-induced ordering of the chains parallel to each other. This argumentation is supported by previous studies concluding that the mesomorphic phase is a transition state of order on the pathway to crystallization for various polyesters and related polymers.[42,56−59,64] However, the present experimental data do not allow confirming whether this imperfectly ordered state is actually nematic liquid-like or not, as suggested by Mulligan and Cakmak.[29] According to Wunderlich et al.'s classification,[71,72] it should belong to the Condis Crystal type, i.e. a crystalline state having high degree of conformational disorder.

Further characterization of the PLA mesomorphic form, and the amorphous state as well, by means of X-ray scattering experiments is in progress regarding a collection of polylactide materials having various concentrations of D-stereoisomer units.

Concluding Discussion

In this work, the evolution with draw temperature of the tensile drawing behavior of amorphous PLA in the rubbery state has been investigated in correlation with the strain-induced structural changes. It was shown that drawing involves a disorder−order transformation for strains exceeding 130%, the degree of order being dependent on the draw temperature. For $T_d < 75$ °C, a mesomorphic ordering of the chains gradually builds up with increasing strain. For $T_d = 80$ °C, the α' crystal form develops in parallel with the mesomorphic form. For $T_d \geq 90$ °C, only the strain-induced α' crystal form is observed up to rupture. Worth noticing is the strong stimulating effect of drawing on the crystallization kinetics as compared with quiescent conditions from either the melt or the glassy state.

The slope of the strain-hardening continuously drops with increasing draw temperature as a result of thermal activation of the plastic deformation. However, the steeper slope of the strain-hardening accompanying the growth of the mesomorphic form at $T_d = 70$ °C is quite surprising as compared with drawing at $T_d =$ 90 °C when α' crystals grow. This is an evidence of the high cohesive energy of the mesomorphic form in spite of its defective ordering.

It has been shown that the occurrence of the strain-induced disorder−order transition is directly correlated with a critical strain and/or orientation of the amorphous chains. It seems that this is a general feature of semicrystalline polymers during hot drawing from the melt, otherwise melt spinning.[73] In the present study, the strain onset of the transition proved to be somewhat higher at $T_d = 90$ °C than at $T_d = 70$ °C due to the higher relaxation capabilities of the chains during the drawing process. This phenomenon is contradictory with previous observation and conclusion by Mulligan and Cakmak[29] regarding the drawing of a polylactide material slightly different from the one of the present work, namely the D-stereoisomer content was 2% and the melting point 165 °C. The shift to lower strain of the strain-hardening onset with increasing draw temperature

was hypothetically ascribed to "the increased role of the thermally activated crystallization". Close examination of the stress−strain plots reported by these authors reveals that the strain-hardening is much more gradual at $T_d < 80$ °C than at $T_d \geq 80$ °C, so that the actual strain onset is not so obvious to determine in the former case. Regarding the present study, the occurrence of thermal crystallization is highly doubtful for several reasons. First, the PLA isothermal crystallization kinetics is clearly inconsistent with thermal crystallization in the time scale of a few minutes for the drawing at temperatures 70 °C $< T_d <$ 90 °C (Figure 2). Second, the fibrillar texturing of the ordered phase, particularly for $T_d = 90$ °C, is a strong hint of the crystallization of highly oriented chains. Third, the drawing at $T_d = 100$ °C confirms that thermal crystallization does not occur in the time scale of the experiments whereas chain relaxation is a highly active process.

Finally, regarding the occurrence of the mesomorphic form, the temperature-dependent chain mobility appears to be a driving force to the strain-induced ordering. However, the contribution of thermodynamics in the process is quite obvious, particularly in consideration of (1) the well-defined X-ray scattering of the mesomorphic form that is relevant of narrow distribution of intermolecular distances and (2) its high cohesiveness that is indicative of strong molecular interactions.

References and Notes

(1) Sinclair, R. G. *J. Macromol. Sci.—Pure Appl. Chem.* **1996**, *33*, 585–597.
(2) Garlotta, D. *J. Polym. Environ.* **2002**, *9*, 63–84.
(3) Auras, R. A.; Harte, B.; Selke, S. *Macromol. Biosci.* **2004**, *4*, 835–864.
(4) Gupta, A. P.; Kumar, V. *Eur. Polym. J.* **2007**, *43*, 4053–4074.
(5) Averous, L. In *Monomers, Polymers and composites from renewable resources*, Belgacem, M. N., Gandini, A., Eds; Elsevier Ltd.: Oxford, U.K.; 2008; pp 433−450.
(6) Tsuji, H.; Ikada, Y. *Macromol. Chem. Phys.* **1996**, *197*, 3483–3499.
(7) Sarasua, J.-R.; Prud'homme, R. E.; Wisniewski, M.; Le Borgne, A.; Spassky, N. *Macromolecules* **1998**, *31*, 3895–3905.
(8) Cartier, L.; Okihara, T.; Ikada, Y.; Tsuji, H.; Puiggali, J.; Lotz, B. *Polymer* **2000**, *41*, 8909–8919.
(9) Ohkoshi, I.; Abe, H.; Doi, Y. *Polymer* **2000**, *41*, 5985–5992.
(10) Park, J. W.; Im, S. S.; Kim, S. H.; Kim, Y. H. *Polym. Eng. Sci.* **2000**, *40*, 2539–2550.
(11) Martin, O.; Averous, L. *Polymer* **2001**, *42*, 6209–6219.
(12) Abe, H.; Kikkawa, Y.; Inoue, Y.; Doi, Y. *Biomacromolecules* **2001**, *2*, 1007–1014.
(13) Pluta, M.; Galeski, A. *J. Appl. Polym. Sci.* **2002**, *86*, 1386–1395.
(14) Ray, S. S.; Maiti, P.; Okamoto, M.; Yamada, K.; Ueda, K. *Macromolecules* **2002**, *35*, 3104–3110.
(15) Ljungberg, N.; Wesslen, B. *Biomacromolecules* **2005**, *6*, 1789–1796.
(16) Kulinski, Z.; Piorkowska, E. *Polymer* **2005**, *46*, 10290–10300.
(17) Tsuji, H.; Takai, H.; Saha, S. K. *Polymer* **2006**, *47*, 3826–3837.
(18) Nam, J. Y.; Okamoto, M.; Okamoto, H.; Nakano, M.; Usuki, A.; Matsuda, M. *Polymer* **2006**, *47*, 1340–1347.
(19) Li, H.; Huneault, M. A. *Polymer* **2007**, *48*, 6855–6866.
(20) Masirek, R.; Piorkowska, E.; Galeski, A.; Mucha, M. *J. Appl. Polym. Sci.* **2007**, *105*, 282–290.
(21) Schwach, E.; Six, J.-L.; Averous, L. *J. Polym. Environ.* **2008**, *16*, 286–297.
(22) Fujimori, A.; Ninomiya, N.; Masuko, T. *Polym. Eng. Sci.* **2008**, *48*, 1103–1111.
(23) Ray, S. S.; Yamada, K.; Okamoto, M.; Ueda, K. *Polymer* **2003**, *44*, 857–866.
(24) Li, Y.; Shimizu, H. *Macromol. Biosci.* **2007**, *7*, 921–928.
(25) Bordes, P.; Pollet, E.; Averous, L. *Prog. Polym. Sci.* **2009**, *34*, 125–155.
(26) Yu, J.; Ai, F.; Dufresne, A.; Gao, S.; Huang, J.; Chang, P. R. *Macromol. Mater. Eng.* **2008**, *293*, 763–770.
(27) Lin, N.; Chen, G.; Huang, J.; Dufresne, A.; Chang, P. R. *J. Appl. Polym. Sci.* **2009**, *113*, 3417–3425.
(28) Kokturk, G.; Serahtkulu, T. F.; Cakmak, M.; Piskin, E. *Polym. Eng. Sci.* **2002**, *42*, 1619–1628.
(29) Mulligan, J.; Cakmak, M. *Macromolecules* **2005**, *38*, 2333–2344.
(30) Ghosh, S.; Vasanthan, N. *J. Appl. Polym. Sci.* **2006**, *101*, 1210–1216.
(31) Stoclet, G.; Elkoun, S.; Miri, V.; Seguela, R.; Lefebvre, J.-M. *Int. Polym. Process.* **2007**, *22*, 385–388.
(32) Pluta, M.; Galeski, A. *Biomacromolecules* **2007**, *8*, 1836–1843.
(33) Ou, X.; Cakmak, M. *Polymer* **2008**, *49*, 5344–5352.
(34) De Sanctis, P.; Kovacs, A. J. *Biopolymers* **1968**, *6*, 299–306.
(35) Hoogsteen, W.; Postmena, A. R.; Pennings, A. J.; Ten Brinke, G.; Zugenmaier, P. *Macromolecules* **1990**, *23*, 634–642.
(36) Zhang, J.; Tashiro, K.; Tsuji, H.; Domb, A. J. *Macromolecules* **2008**, *41*, 1352–1357.
(37) Eling, B.; Gogolewski, S.; Pennings, A. J. *Polymer* **1982**, *23*, 1587–1593.
(38) Puiggali, J.; Ikada, Y.; Tsuji, H.; Cartier, L.; Okihara, T.; Lotz, B. *Polymer* **2000**, *41*, 8921–8930.
(39) Fischer, E. W.; Sterzel Hans, J.; Wegner, G. *Kolloid Z. Z. Polym.* **1973**, *21*, 980–990.
(40) Jamshidi, K.; Hyon, S.-H.; Ikada, Y. *Polymer* **1988**, *29*, 2229–2234.
(41) Murthy, N. S.; Correale, S. T.; Minor, H. *Macromolecules* **1991**, *24*, 1185–1189.
(42) Fu, Y.; Busing, W. R.; Jin, Y.; Affholter, K. A.; Wunderlich, B. *Macromol. Chem. Phys.* **1994**, *195*, 803–822.
(43) Wu, J.; Schultz, J. M. *Polymer* **2002**, *43*, 6695–6700.
(44) Le Bourvelec, G.; Monnerie, L.; Jarry, J. P. *Polymer* **1986**, *27*, 856–860. Le Bourvelec, G.; Monnerie, L.; Jarry, J. P. *Polymer* **1987**, *28*, 1712–1716.
(45) Lapersonne, P.; Bower, D. I.; Ward, I. M. *Polymer* **1992**, *33*, 1277–1283.
(46) Capaccio, G.; Ward, I. M. *J. Polym. Sci., Polym. Phys.* **1984**, *22*, 475–484The drawing behavior of polyethylene copolymers.
(47) Duffo, P.; Monasse, B.; Haudin, J.-M.; G'Sell, C.; Dahoun, A. *J. Mater. Sci.* **1995**, *30*, 701–711.
(48) Djezzar, K.; Penel, L.; Lefebvre, J.-M.; Seguela, R.; Germain, Y. *Polymer* **1998**, *39*, 3945–3953.
(49) Penel-Pierron, L.; Seguela, R.; Lefebvre, J.-M.; Miri, V.; Debecker, C.; Jutigny, M.; Pabiot, J. *J. Polym. Sci., Polym. Phys.* **2001**, *39*, 1224–1236.
(50) Matsushige, K.; Nagata, K.; Imada, S.; Takemura, T. *Polymer* **1980**, *21*, 1391–1397.
(51) Mahendrasingam, A.; Blundell, D. J.; Parton, M.; Wright, A. K.; Rasburn, J.; Narayanan, T.; Fuller, W. *Polymer* **2005**, *46*, 6009–6015.
(52) Mitchell, G. R.; Lovell, R. *Acta Crystallogrt.* **1981**, *A37*, 189–196.
(53) Sun, T.; Zhang, A.; Li, F. M.; Porter, R. S. *Polymer* **1988**, *29*, 2115–2120.
(54) Parravicini, L.; Leone, B.; Auriemma, F.; Guerra, G.; Petraccone, V.; Di Dino, G.; Bianchi, R.; Vosa, R. *J. Appl. Polym. Sci.* **1994**, *52*, 875–885.
(55) Carr, P. L.; Nicholson, T. M.; Ward, I. M. *Polym. Adv. Technol.* **1997**, *8*, 592–600.
(56) Welsh, G. E.; Blundell, D. J.; Windle, A. H. *Macromolecules* **1998**, *31*, 7562–7565. Welsh, G. E.; Blundell, D. J.; Windle, A. H. *J. Mater. Sci.* **2000**, *35*, 5225–5240.
(57) Mahendrasingam, A.; Martin, C.; Fuller, W.; Blundell, D. J.; Oldman, R. J.; McKerron, D. H.; Harvie, J. L.; Riekel, C. *Polymer* **2000**, *41*, 1217–1221.
(58) Ran, S.; Wang, Z.; Burger, C.; Chu, B.; Hsiao, B. S. *Macromolecules* **2002**, *35*, 10102–10107.
(59) Mahendrasingam, A.; Blundell, D. J.; Martin, C.; Urban, V.; Narayanan, T.; Fuller, W. *Polymer* **2005**, *46*, 6044–6049.
(60) Pellerin, C.; Pezolet, M.; Griffiths, P. R. *Macromolecules* **2006**, *39*, 6546–6551.
(61) Cakmak, M.; Lee, S. W. *Polymer* **1995**, *36*, 4039–4054.
(62) Jakeways, R.; Klein, J. L.; Ward, I. M. *Polymer* **1996**, *37*, 3761–3762.
(63) Garcia-Gutierrez, M. C.; Karger-Kocsis, J.; Riekel, C. *Macromolecules* **2002**, *35*, 7320–7325.
(64) Wu, J.; Schlutz, J. M.; Samon, J. M.; Pangelinan, A. B.; Chuah, H. H. *Polymer* **2001**, *42*, 7141–7151.
(65) Konishi, T.; Nishida, K.; Matsuba, G.; Kanaya, T. *Macromolecules* **2008**, *41*, 3157–3161.
(66) Aharoni, S. M.; Correale, S. T.; Hammond, W. B.; Hatfield, G. R.; Murthy, N. S. *Macromolecules* **1989**, *22*, 1137–1141.
(67) Seguela, R. *J. Macromol. Sci., Polym. Rev.* **2005**, *45*, 263–287.
(68) Xiao, C.; Jho, J. Y.; Yee, A. F. *Macromolecules* **1994**, *27*, 2761–2768.
(69) Alberola, N. D.; Mele, P.; Bas, C. *J. Appl. Polym. Sci.* **1997**, *64*, 1053–1059.

(70) Blundell, D. J.; Mahendrasingam, A.; Martin, C.; Fuller, W.; MacKerron, D. H.; Harvie, J. L.; Oldman, R. J.; Riekel, C. *Polymer* **2000**, *41*, 7793–7802.
(71) Wunderlich, B.; Grebowicz, J. *Adv. Polym. Sci.* **1984**, *60/61*, 1–61.
(72) Wunderlich, B.; Möller, M.; Grebowicz, J.; Bauer, H. *Adv. Polym. Sci.* **1988**, *87*, 1–137.
(73) Samon, J. M.; Schultz, J. M.; Hsiao, B. S. *Polymer* **2002**, *43*, 1873–1875.